Barriers to Hydride Transfer in Wild Type and Mutant Dihydrofolate Reductase from *E. coli*

Ian F. Thorpe and Charles L. Brooks, III*

Department of Molecular Biology (TPC6), Center for Theoretical Biological Physics, The Scripps Research Institute, 10550 North Torrey Pines Road, La Jolla, California 92037

Received: June 18, 2003; In Final Form: October 6, 2003

We have calculated the distribution of activation energies for the key hydride transfer step in the reduction of dihydrofolate by the enzyme dihydrofolate reductase in wild-type DHFR as well as the G121S and G121V variants of the *Escherichia coli* enzyme using combined quantum mechanical/molecular mechanical methods. Comparison of the activation energy distributions present in the three protein systems demonstrates that the ensemble of energy barriers differs in each. The features of these energy barrier distributions are consistent with experimentally determined reaction rates for the three proteins and support experimental observations demonstrating time-dependent variation in the reaction rate of individual enzyme molecules. This occurrence suggests that several distinct conformational substates in the proteins modify the potential energy surface for the reaction. A select set of distances and dihedral angles was observed to correlate well with the progress of the reaction or with the presence of protein conformations giving rise to low reaction barriers. These geometric parameters highlight features in the wild-type and mutant conformational ensembles that may give rise to the observed energy distributions. Our work demonstrates that these structural probes are indicators of changes in the equilibrium properties of the enzyme systems studied; they do not appear to arise as the result of direct coupling of time-dependent protein displacements to the reactive event.

1. Introduction

The enzyme dihydrofolate reductase (DHFR) catalyzes the reduction of 7,8-dihydrofolate (DHF) to 5,6,7,8-tetrahydrofolate (THF) utilizing the nucleotide cofactor NADPH (Figure 1a).[1] The reduction of DHF is initiated through protonation at the N5 position,[2] possibly mediated by the residue ASP 27 via one or more intermediate water molecules in the active site.[3] Because of this protonation step, the reaction exhibits pH dependent kinetics ($pK_a = 6.5$).[4] Protonation at the N5 position is followed by the transfer of a hydrogen atom from NADPH to $DHFH^+$. The hydrogen is generally thought to undergo the translocation as a hydride ion.[5]

DHFR has been extensively studied using a variety of both experimental[4,6−8] and computational techniques.[9−12] Crystallographic studies on several DHFR complexes indicate that several structural changes occur throughout the reaction cycle of the enzyme. Among these are modulations in the conformation of the Methionine-20 (M20) loop (residues 14−24). This loop abuts the site of chemistry within the enzyme and is thought to play a crucial role in the binding of the cofactor and substrate to DHFR (Figure 1).[13] Mutational studies have identified amino acid residues that, while located far away from the active site (up to 19 Å), have an effect on the catalytic activity of the enzyme when altered. A case in point is the residue glycine-121. This residue is approximately 19 Å from the site of chemistry in DHFR (Figure 1b). However, changing this residue to valine (G121V) causes a 200-fold reduction in the hydride-transfer rate. This mutation modifies the kinetic cycle of DHFR, necessitating an additional conformational change in the protein that can be detected through kinetic experiments.[14] Changing residue 121 to serine (G121S) also reduces the hydride-transfer rate. An additional conformational change is not seen in the serine mutant, suggesting that the conformational ensemble of

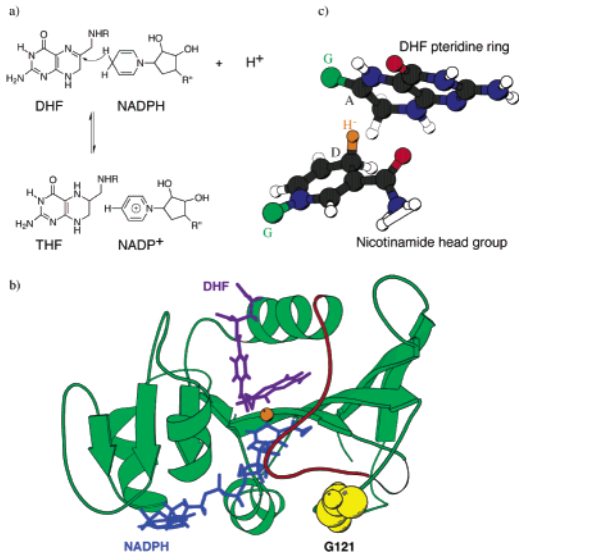

Figure 1. (a) The reaction catalyzed by DHFR. (b) A molecular diagram of wild-type DHFR before hydride transfer. The ligands DHF and NADPH are indicated by atomic detail, the orange sphere between them corresponds to the hydride transferred. The M20 loop is displayed in red while glycine residue 121 is represented by yellow van der Waals spheres. The figure was generated using the MolScript program[17] and the X-ray coordinates 1rx2.[13] (c) The quantum mechanical region employed for hydride-transfer energy calculations includes all atoms shown. The positions denoted G, A, D, H^- represent GHO boundary atoms, acceptor and donor carbons, and hydride, respectively (see section 2.2).

* Corresponding author. Phone: 858/784-8035; fax: 858/784-8688; e-mail: brooks@scripps.edu.

10.1021/jp035734n CCC: $25.00
Published on Web 11/20/2003

this mutant is more similar to that of wild-type DHFR than the valine mutant. It is unclear how distant mutations at a single site could effect the rate of hydride transfer and the conformational ensemble of the protein in such markedly different ways. However, in theoretical studies of this system, Brooks and coworkers have observed that sequentially and spatially distant residues are coupled, undergoing correlated motions in the ternary complexes of native and mutant DHFRs containing reactive species NADPH and DHF and that the extent of coupling diminishes with diminished efficacy of hydride transfer, suggesting some "communication" between reaction center atoms and distant residues (see Radkiewicz and Brooks[15] and Rod et al.[16]).

At least three different mechanisms could accommodate the observation that sequence and spatially distant residues modulate chemistry in the active site. In the first, the correlated motions affect the reaction rate by modulating the conformational ensemble, selecting conformations of the ligands that are amenable to the progress of the reaction. These conformations are already part of the conformational ensemble when the ligands are unbound, but the process of binding to the enzyme increases their population. One established view is that the catalytic activity of enzymes is due primarily to such preorganization.[18] In this hypothesis, prearranging reactive groups in the active site of the enzyme negates large entropic penalties because of reorganization of the reactants into transition-state conformations. In a second mechanism, the protein environment causes the development of new fluctuations in the ligands that do not occur if the ligands are unbound.[19] In contrast to the first mechanism, where the ligands are restricted to specific parts of the potential energy surface when bound, the underlying potential energy surface itself is modified in this model. In a third mechanism, specific motions could directly act to facilitate the reactive event. Many enzymes are flexible and are subject to fluctuations on a broad range of time scales. Consequently, it has been theorized that specific modes of motion in the protein may play a key role in reducing the energy barrier for an enzyme-catalyzed reaction by coupling directly to the reaction coordinate.[20,21] This definition of "promoting" motions could include the influence of both equilibrium and dynamic effects.[22] We seek to distinguish between these two possibilities. The former only requires that the equilibrium ensembles generated by fluctuations of the enzyme be present. We consider such an effect to be more appropriately defined as the influence of preorganization on the system. The contribution of protein motion in the latter context explicitly requires the time-dependent displacements of enzymatic groups. Henceforth, we shall refer to the impact of such time-dependent displacements on enzymatic reactions as dynamic coupling.

We can investigate the relative importance of these three mechanisms in mediating rate differences between wild-type and mutant DHFR by examining equilibrium ensembles of hydride-transfer barriers as well as the distributions of structural parameters present in the different protein isoforms. If changes in the efficacy of preorganization are the primary source of lowered reactivity in mutants, the range of activation energies need not be significantly different for specific mutant and wild-type enzyme conformations, only the distributions of conformations need change. However, if unique protein fluctuations are the source of rate differences between wild-type DHFR and mutants, both the conformations sampled and the range of reaction barriers present would vary among the wild-type and mutant proteins. The absence of either differences in the conformational ensembles or reaction barrier distributions would suggest that the source of the rate differences is dynamic coupling as defined above.

As reported in the literature, reaction rates at neutral pH for wild-type DHFR ($\approx$220 s^{-1}) and G121V ($\approx$1.3 s^{-1}) are consistently similar while that of G121S varies in the three papers published containing these data (40.1 s^{-1} and 3.7 s^{-1} in Cameron and Benkovic 1997,[14] Agarwal et al. 2002,[23] and Rajagopalan et al.[24]). The macroscopic rate constant for hydride transfer, k, may be related to the free-energy barrier for this process through the usual transition-state theory expression as $k = k_0 \cdot \exp[-\Delta G^{\ddagger}/k_B T]$. Assuming k_0 is constant between mutants, the relative reaction rates can be used to derive differences in the activation free energy of the wild-type protein and the two mutants. A value of approximately 3 kcal/mol is obtained for the activation free-energy difference between wild-type DHFR and G121V ($\Delta\Delta G^{\ddagger} = 3$ kcal/mol). For G121S, $\Delta\Delta G^{\ddagger}$ is either 1 or 2.4 kcal/mol compared to wild type for the experimentally measured hydride-transfer rates of 40.1 s^{-1} and 3.7 s^{-1} respectively. Despite the discrepancy between the measured rates for G121S, we expect to see a larger difference between wild type and G121V hydride-transfer barriers than between wild type and G121S.

Earlier theoretical studies have indicated that certain correlated fluctuations in DHFR are unique to the reactive ternary complex DHFR:NADPH:DHF.[15] We posit that the long-range affect of mutations at position 121 is mediated by differences in these fluctuations as represented by equilibrium structural ensembles present in the three protein systems. However, it has been suggested by other researchers that the time-dependent displacements of groups within an enzyme can facilitate hydride transfer.[20−22] Consequently, we desired to test whether changes in patterns of correlated motion observed in DHFR reflect such dynamical coupling of protein fluctuations to the height of the hydride-transfer barrier in the enzyme. In other words, we sought to investigate whether the direct involvement of time-dependent displacements of the protein is necessary to account for the differences in the efficacy of the hydride-transfer step in DHFR and the G121V and G121S mutants.

To test this hypothesis, we calculated the distribution of hydride-transfer barriers corresponding to fixed protein systems taken from molecular dynamics (MD) trajectories. The effective activation free energies calculated from the distributions of hydride-transfer barriers are in qualitative agreement with experimentally determined reaction rate differences between the proteins. In addition to demonstrating that ensembles of hydride-transfer barriers present in the wild-type and mutant proteins differ, these results show that the changes in distributions of hydride-transfer barriers in DHFR predominantly reflect changes in the equilibrium ensemble of protein conformations.

Evidence for a network of coupled motions that correlate with the course of the reaction in DHFR and the G121V mutant has recently been presented by Hammes-Schiffer and co-workers.[12,23,25] In these studies, information about thermally averaged geometric properties that may be related to the reactive event were computed. These researchers were unable to determine whether changes in protein conformation modulate the reactive event or whether structural changes in the protein stem from rearrangements in the reactive center. We explore this question further.

To do this, we used the same fixed protein systems we employed to calculate effective hydride-transfer barriers above and examined many of the geometric parameters that Hammes-Schiffer and co-workers found to be associated with progress along the reaction coordinate in wild-type DHFR.[12,23] The results

of this procedure exhibit qualitative agreement with the work of these authors despite the fact that we employed a static protein environment. This reveals that changes in the previously identified geometric parameters stem from the course of the catalytic event itself and do not have their origin in fluctuations of the protein. This observation also demonstrates that changes in these parameters are not the result of direct coupling of time-dependent displacements of enzymatic groups to the reactive process.

In addition to the distances presented by Hammes-Schiffer and co-workers, we observed that a select set of backbone ϕ and ψ angles correlated with the presence of protein conformations giving rise to low-hydride-transfer barriers. Our findings indicate that the instantaneous reaction barrier for hydride transfer in DHFR varies with time. From a fluctuating energy barrier for the hydride transfer, we infer a reaction rate that also varies with time. This observation agrees with the results of experimental[26] and computational[27] studies identifying time-dependent reaction rates for individual enzyme molecules.

2. Methods

2.1. Selection of Structures. The initial protein structures were derived from a crystal structure of *E. coli* DHFR complexed to folate and $NADP^+$ (PDB identifier 1rx2).[13] The structures of NADPH and DHF were obtained by making modifications to this structure as described previously.[15] The G121V and G121S mutants were generated by computationally converting residue 121 to valine or serine and employing parameters of the CHARMM[28] force field to determine the coordinates of missing atom positions. Following the modifications, the energy of the proteins was minimized using harmonic restraints. No large-scale structural or energetic changes in the resulting proteins were observed. The proteins were then solvated in truncated octahedra composed of 3000−5000 TIP3P water molecules.[29] Molecular dynamics simulations of the ternary Michaelis complex for the three enzyme systems were carried out at a temperature of 298 K using the CHARMM molecular mechanics program.[30] Aspartate 27, a residue previously thought to play a key role in generating an environment favorable to protonation of DHF[3], was unprotonated. A van der Waals switching function between 8 and 11 Å, a shifting function for the electrostatic interactions with a cutoff of 11 Å, a nonbonded cutoff of 13 Å, and periodic boundary conditions were utilized in all MD simulations. After an equilibration period of 100 ps, these simulations were extended to 10 ns. A time step of 0.002 ps was employed and snapshots saved every 200 steps. Simulation protocols are identical to those reported previously by Radkiewicz and Brooks.[15]

From these trajectories, snapshots were identified in which the distance between the transferred hydrogen and the acceptor carbon was less than or equal to 2.5 Å. According to other QM/MM calculations, this distance is approximately 1.5 Å at the transition state.[31,32] However, the empirical energy terms employed in MD simulations do not permit such close approaches to occur. The distance chosen is one that represents relatively close approach of the transferred hydrogen to the carbon acceptor of the pterin ring and generates an ensemble of structures of manageable size. Selection based on this criterion yielded ensembles of 834, 394, and 607 structures for the wild type, G121S, and G121V systems, respectively. Since the configurations were taken from MD simulations that evolved in a time-dependent manner, a subset of these structures well dispersed in time was selected for analysis of hydride-transfer barriers. This was done to ensure that snapshots investigated represent a diverse set of protein and solvent configurations. This procedure resulted in 284, 190, and 299 structures for the wild type, G121S, and G121V systems. These snapshots provide a representative sample from the trajectories while limiting the investigation to relevant structures: those with the closest approach of the transferred hydrogen to the acceptor carbon.

2.2. Calculation of the Hydride-Transfer Barrier Using QM/MM Methods. In the QM/MM approach, a quantum mechanical (QM) description is employed for a small region of interest within the system being studied, allowing the charge transfer that accompanies bond breaking and formation to be adequately described.[33] The remainder of the system is represented by the fixed charges and empirical potentials of a molecular mechanics (MM) force field. In our studies, the PM3 semiempirical method is employed to describe the QM region. In employing this approach, our goal was not to reproduce experimentally derived values. Neither semiempirical methods nor classical force fields are necessarily capable of generating results of chemical accuracy for reaction barriers in enzymes. However, these methods are robust in predicting trends of the properties associated with molecular systems. Moreover, the hydride-transfer reaction that is the subject of this work is well within the scope of reactions that semiempirical methods were originally parametrized to represent and for which they have been widely used.[32,34,35] Thus, we believe it is possible to employ this methodology to make meaningful comparisons between energetic features identified in the mutant and wild-type proteins to gain insight regarding the qualitative nature of the differences present in these systems.

To initiate our studies, a sphere of radius 30 Å around the transferred hydride was isolated from the snapshots identified above; this included all of the protein and much of the solvent. A proton was then added to the DHF ligand at position N5 using the HBUILD facility in CHARMM. This generated the reactive precursor $DHFH^+$ to which the final hydride is transferred. Upon addition of this proton, the protein formal charge changed from −17 to −16. Theoretical studies by Gready indicate that protonation of DHF prior to hydride transfer greatly facilitates the transfer process.[36] Additionally, Raman spectroscopy studies by Chen et al. indicate that the pK_a of N5 in DHF is approximately 6.5 in a ternary complex which the authors considered to be an appropriate model for the wild-type Michaelis complex.[37] This strongly suggests that a significant fraction of DHF in the wild-type ternary complex is protonated at position N5 at pH 7, the pH at which the kinetic experiments characterizing the hydride-transfer rate of wild-type DHFR, G121S, and G121V were done.[14,23] These results were corroborated by theoretical calculations from Rod and Brooks[2] and from Deng and Callendar.[38] The latter group calculated Raman frequency shifts corresponding to those measured by Chen et al. An analysis by these authors concluded that a mechanism in which protonation precedes hydride transfer agrees best with the available theoretical and experimental data. The MD simulations were not carried out for the protonated Michaelis complex. However, while it must exist because of the demands of chemistry, the ternary Michaelis complex DHFR:NADPH:DHFH+ has never been directly observed experimentally. The reaction proceeds to completion without the detection of intermediates; it progresses so swiftly that protonated DHF must be a transient species in the Michaelis complex relative to the equilibrium fluctuations of DHFR. However, for $DHFH^+$ to have a significant impact on the equilibrium fluctuations of DHFR, this species must have an appreciable lifetime. As noted earlier, correlated motions are observed for the reactant ternary

DHFR:NADPH:DHF complex, but not for the corresponding product ternary complex DHFR:NADP:THF.[15] Without experimental evidence for an appreciable lifetime for $DHFH^+$ in the reactant ternary complex, we anticipate that protonation of DHF represents a small perturbation (i.e., within the linear response regime) on the fluctuations observed when unprotonated DHF is present. As such, it is reasonable to employ snapshots from these trajectories as starting points for our QM/MM calculations. This point was recently verified by work from Rod and Brooks,[2] who showed that the pK_a value for the N5 position was independent of whether the calculations were performed on the basis of simulations of DHFR:NADPH:DHF or DHFR:NADPH:DHF^+.

Certain MM atoms within the ligands DHF and NADPH were reassigned as QM atoms, generating the QM regions shown in Figure 1c, where G are GHO boundary atoms.[39] GHO atoms are link atoms at the boundary of the QM and MM regions and are added as part of the QM/MM methodology in CHARMM.[30] In DHFR, the time scale for the actual hydride-transfer event should be on the order of the time scale of a bond vibration (a few picoseconds) because of the short distance traveled by the hydride (~1 Å). The structure of the protein is not likely to undergo large-scale rearrangement during this time. Consequently, the protein environment in the simulation was kept fixed and only the two ligands and solvent atoms within 10 Å of the transferred hydride were allowed to move in response to hydride translocation. The distance between the transferred hydride and the acceptor carbon was systematically decreased until the hydride-donor carbon bond was broken and a new bond to the acceptor formed. Each reaction path was composed of 36 nonequidistant points. The distance between each point ranged from a maximum of 0.1 Å early in the reaction path to a minimum of 0.055 Å in the region of the transition state. The energy of all mobile atoms was minimized at each point until a tolerance of 0.001 kcal/(mol·Å) in the energy gradient was achieved. Minimization was carried out using the Adopted Basis Newton−Raphson minimization routine in CHARMM. The calculations for each point took between 30 and 60 min to complete on an SGI Origin 3800 processor. The energy barrier was determined as the difference between the highest energy obtained along the reaction path and the initial energy of the system. This procedure generates minimum energy paths for the hydride-transfer reaction in the context of diverse protein environments. This approach is similar in spirit to that of other researchers employing QM/MM methods to study enzyme catalyzed reactions.[22,27]

Because MD simulations represent thermal ensembles corresponding to a canonical distribution (or isothermal−isobaric under constant T and P), we can employ subsets of structures from these simulations to calculate the activation free energy for the hydride transfer following the free-energy perturbation approach.[40] Thus, from our ensemble of protein conformations for each mutant we compute the energy change needed to alter the system conformation to the transition state for hydride transfer (using the QM/MM approach just described) and then construct the free-energy barrier for hydride transfer in each system from the straightforward connection formula

$$\exp(-\Delta G^{\ddagger}/k_B T) = \langle \exp(-\Delta E^{\ddagger}/k_B T)\rangle_R = \frac{1}{N}\sum_m \exp(-\Delta E_m{}^{\ddagger}/k_B T) = \sum_l P(\Delta E_l^{\ddagger}) \exp(-\Delta E_l^{\ddagger}/k_B T) \quad (1)$$

where the subscript R denotes that the average is taken over the ensemble of conformations (N) generated from our simulations of the Michaelis complexes, $\Delta E^{\ddagger}$ corresponds to the difference between the first point and the highest energy point along the hydride-transfer path and $P(\Delta E^{\ddagger})$ is the histogram (or probability distribution) of calculated barrier heights. The sum over states from the simulation (2nd equality in eq 1) or the corresponding sum over the distribution of energy barriers constructed from the simulation (3rd equality in eq 1) are identical representations of the average denoted by the first equality in eq 1. Also, substitution of a constant prefactor, k_0, in front of these expressions shows how the microscopic distribution of barriers is related to the microscopic distribution of barrier-crossing rates observed in single-molecule experiments and how thermal averaging over this distribution is related to the macroscopically observed rate constant, assuming that the same prefactor is applicable to all of the sampled reaction environments.[26,41]

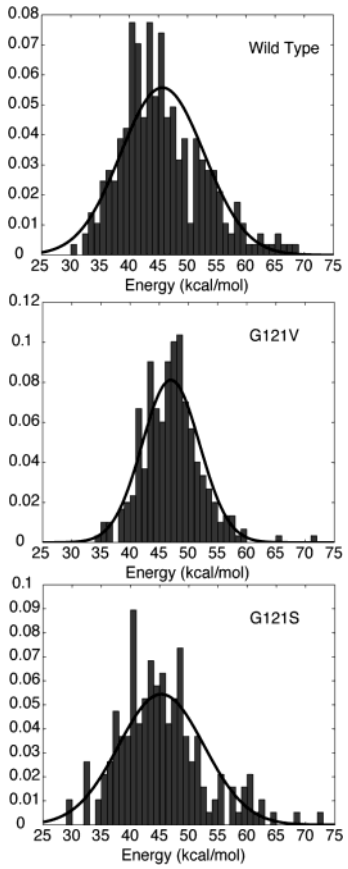

Figure 2. Histograms of calculated hydride-transfer energy barrier distributions for (a) wild type, (b) G121V, and (c) G121S enzymes. The lines represent a Gaussian fit to the data.

We carried out this procedure by constructing histograms of the hydride-transfer energy barriers for the three enzyme systems. The resulting normalized histograms (probability distributions) of energy barriers can be used directly in eq 1. A consequence of the averaging procedure described by eq 1 is that activation energy barriers on the leading edge of the distribution have a greater impact on the free-energy barrier than do higher energy barriers. However, because of the low occurrence of these small barriers (see Figure 2), we are less confident that they are sampled adequately. Insufficient sampling in these regions could influence the calculated free-energy barriers. This motivated our use of a Gaussian approximant to model each distribution. By using an analytical form for this distribution, we reduce the effects from random noise on the data. In addition, while we expect barriers at either extreme of the distribution to be inadequately sampled because they occur

infrequently, we expect reasonable estimates of the mean and variance of the distributions to emerge relatively quickly from the calculations. Thus, by deriving the parameters for the Gaussian approximant directly from the observed mean and variance of the energy barrier distributions, we are better able to explore the critical tail regions of these distributions. We determined the mean and standard deviation of each energy distribution and constructed $P_x(\Delta E^{\ddagger})$ according to

$$P_x(\Delta E^{\ddagger}) = \frac{1}{\sigma_x\sqrt{2\pi}}\exp\left(-\frac{(\Delta E^{\ddagger} - <\Delta E^{\ddagger}>_x)^2}{2\sigma_x}\right) \qquad (2)$$

where $P(\Delta E^{\ddagger})$ is the probability of observing an energy barrier $\Delta E^{\ddagger}$ for species x, σ_x is the variance of energy barrier distribution x, and $<\Delta E^{\ddagger}>_x$ is the average value of the energy barrier for species *x*. Values of $\Delta E^{\ddagger}$ range from 0 to 100 kcal/mol and x is the wild type, G121V, or G121S proteins.

It is well known that semiempirical methods tend to overestimate reaction barriers (for example, see Garcia-Viloca et al.[42]). To asses this error for our system, we employed the following procedure. Several energy profiles resulting from the semiempirical QM/MM procedure described above were selected and for each step in the profile the entire MM portion of the system was deleted and the GHO boundary atoms were replaced by hydrogen atoms. The resulting molecular system was then subjected to single-point vacuum calculations employing PM3 semiempirical theory, B3LYP density functional theory, and MP2 Hartree−Fock theory. PM3 calculations were carried out using the CHARMM program. B3LYP and MP2 results were generated from the Gaussian 98 program[43] using the 6-311++(d,p) basis set and SCF convergence criteria of 10^{-8} on the density.

2.3. Backbone Dihedral Comparisons. Visual inspection of snapshots with high or low hydride-transfer barriers indicated that the hydrophobic core and associated secondary structural elements of DHFR were nearly identical regardless of the conformation examined. Therefore, we chose to investigate whether changes of the protein backbone in one of the several loop regions (14−24, 60−72, 119−124, 132−139, 142−150) correlated with the occurrence of high or low barriers. Several other regions in the structures suggested to have an impact on the reaction rate via experimental[7] and computational[23] studies were also included. The ϕ and ψ dihedral angles for these residues were recorded and grouped using the ART-2 clustering algorithm implemented in CHARMM.[44] ART-2 is an optimal clustering algorithm based on a self-organizing neural net. The algorithm incorporates an iterative minimization procedure to minimize the Euclidian distance between a cluster center and its members. During the process, a user-defined cluster radius ensures that no member of a cluster is further than the specified Euclidean distance from the cluster center. In each case, this clustering radius was defined so as to generate distinct, well-separated groups. The resulting clusters were interrogated to assess whether certain ϕ/ψ patterns were found preferentially in structures giving rise to either low or high hydride-transfer barriers.

3. Results

3.1. Energetic Barriers to Hydride Transfer. Histograms of the energy distributions obtained can be seen in Figure 2, along with the corresponding normalized Gaussian distributions calculated according to eq 2 above. This ensemble contains the structures (those with the closest hydrogen−acceptor distances) that, on average, should give rise to the lowest energy barriers for hydride transfer. We anticipate that structures containing longer hydrogen−acceptor distances result in barriers to hydride transfer that are significantly higher than those found in the low end of each distribution. Because of the form of eq 1, the contribution of individual barriers greater than ∼50 kcal to each free-energy barrier is negligible. Such structures would have to be exponentially more abundant than the low barrier states we have identified to significantly impact the free-energy barrier. Given that our MD trajectories satisfy quasi-ergodicity and that we have sampled ∼1% of these trajectories in generating the ensembles of hydride-transfer barriers, this is highly unlikely. The wide range of energy barriers obtained, despite the similar distance criterion employed in the selection of each snapshot, demonstrates that in addition to the hydrogen−acceptor distance the barrier to hydride transfer is impacted by environmental features. In fact, the hydride-transfer barrier must be a function of the entire protein and solvent configuration, as these are the only things that vary significantly between different snapshots. The energy distributions approximate the Gaussian curves, the anticipated appearance for a thermally distributed ensemble of energy barriers. The activation free energies for the wild type, G121S, and G121V distributions are 13.7, 12.9, and 26.6 kcal/mol, respectively (see Table 1).

TABLE 1: Hydride-Transfer Barriers in DHFR

enzyme	calculated ΔG^a (kcal/mol)	calculated $\Delta\Delta G^a$ (kcal/mol)	measured $\Delta\Delta G^b$ (kcal/mol)
wild type	13.7 (33.4)		
G121S	12.9 (32.0)	−0.8	1[c]/2.4[d]
G121V	26.6 (37.6)	12.9	3.0[c,d]

[a] Values in parentheses correspond to estimated barriers from eq 1 without Gaussian approximant to $P_x(\Delta E^{\ddagger})$. [b] Determined using the ratio of the experimental hydride-transfer rates of mutant DHFR with the wild-type protein at 298 K. [c] Reported by Cameron et al.[14] [d] Reported by Rajagopalan et al.[24]

3.2. Geometric Descriptors of Hydride Transfer in DHFR. A set of representative distances that may correlate with the progress of hydride transfer is displayed in the Appendix, Table A1, along with the same data from calculations by Hammes-Schiffer and co-workers.[12] While smaller in magnitude, the percent change that we observe for these distances is generally of the same sign as that reported in the earlier study. In some instances, however, the differences between the two sets of results can be substantial. The significance of these cases is discussed in detail below. Several distances are strongly correlated with progress along the reaction coordinate, including those between the acceptor carbon and each of the donor carbon, Phe31Cζ and Tyr100OH. Representative figures illustrating how changes in the average value of certain geometric parameters vary with hydride-transfer progress are presented in Figure 3. The distance between the donor and acceptor atoms defines the reaction coordinate. Consequently, the change in this distance is very similar among the three enzyme variants. Figure 3b and c highlight differences in these geometric parameters for the three protein systems. Both the shape of the curves and the length scales involved are altered. There are also other geometric features that exhibit such behavior among the three proteins. These features highlight differences in the wild type and mutant conformational ensembles that may be the origin of the observed energy distributions and corresponding variations in rate among the three protein systems.

4. Discussion

4.1. Equilibrium Distributions of Hydride-Transfer Barriers. Our results establish that the energy barrier for hydride

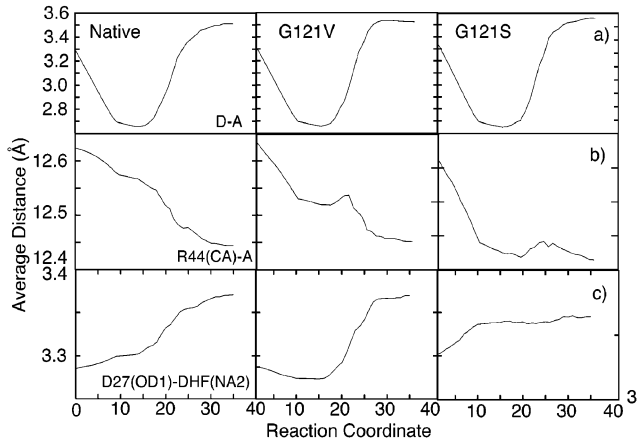

Figure 3. Variation of average distances between specified atoms in wild-type, G121S, and G121V enzymes. In panel (a) D = donor carbon and A = acceptor carbon. Atom names in panels (b) and (c) correspond to PDB names for the atom types. These plots were generated by averaging the distances between the specified atoms over all structures for each point along the reaction path. Note the scale change between the first two panels in row c and the third.

transfer in DHFR varies throughout the time course of the MD simulations. A fluctuating energy barrier indicates that the instantaneous rate of the chemical reaction also varies with time. Time-dependent energy barriers for an enzyme-catalyzed reaction have been demonstrated in the very recent computational studies of Zhang et al.[27] and experimentally by Lu et al.[26] This time-dependent variation in reaction rate was attributed to slow conformational changes in the protein by the latter researchers. Theoretical analyses reveal that such observations are consistent with the presence of two or more protein conformers with distinct reaction rates.[45] The simulations that are the basis of our study are analogous to the single molecule experiments done by Lu et al. We believe the variation in hydride-transfer barriers that we observe is derived from a similar mechanism in DHFR. This issue was first discussed by Frauenfelder et al., who introduced the concept of multiple protein substates to describe the phenomenon.[46] The topic was further elaborated by Wang and Wolynes, who employed a generalized reaction diffusion description to characterize these processes.[47] In such models, multiple conformations of an enzyme molecule can each give rise to separate energy barriers for the reaction it catalyses. The rate for individual enzymes may vary with time as well as between different enzyme molecules. The experimentally measured rate, averaged over a large ensemble, is thus a consequence of these two factors.

In calculating activation free energies, we have employed the microscopic energy barriers derived from ensembles of structures for each protein to compute a thermally averaged reaction barrier comparable to what is measured via traditional experimental techniques. There has been recent work to characterize the behavior of single DHFR molecules.[48] We look forward to further developments in this area, as such experiments are analogous to our computational studies and should allow for direct comparisons with our work.

The individual energy barriers calculated in this study are too high for a reaction on the millisecond time scale, as determined via transition-state theory. Employing the intrinsic hydride-transfer rate of 950 s^{-1} reported for the wild-type enzyme,[4] the transition-state theory expression (see Introduction) predicts an activation free energy for the hydride transfer of close to 13.4 kcal/mol, while our distributions of microscopic energy barriers range from 30 to 75 kcal/mol. However, these

TABLE 2: Comparison of Single-Point Vacuum Energy Profiles for Randomly Selected MD Snapshots

snapshot identifier	$\Delta E^{\ddagger}$ (kcal)[a]		
	PM3	B3LYP	MP2
192	33.5	11.5	10.5
256	51.0	35.0	32.0
345	54.3	37.0	37.0
351	35.9	16.1	12.8

[a] $\Delta E^{\ddagger}$ is defined as the difference between the initial point and the highest energy point in each energy profile.

computed values are in good agreement with the results of other researchers employing semiempirical methods to study similar reactions.[32,49] To estimate the order of the error due to the PM3 method itself, we compared vacuum PM3 single-point calculations to similar calculations at higher levels of theory for models of the QM region taken from different MD snapshots. This effort was similar in spirit to the recent work of other researchers who sought to determine the intrinsic error due to PM3 for the hydride transfer in DHFR.[50] Our calculations indicate that PM3 overestimates the energy barrier for this reaction by 10−20 kcal/mol relative to calculations employing the B3LYP functional or MP2 Hartree−Fock theory (Table 2). When one considers that PM3 overestimates individual hydride-transfer barriers, the free-energy differences that we compute are in reasonable qualitative agreement with our expectations on the basis of the experimentally determined rate constants (Table 1). The results presented in Table 2 also indicate that the error due to PM3 is systematic (i.e., it always overestimates the barrier) across the different MD snapshots employed for our calculations. This gives us confidence that the observations we have made regarding the relative ordering of the calculated free energies are robust.

4.2. Relevance of Free-Energy Hydride-Transfer Barriers to Experimentally Measured Rate Constants. The free-energy barrier obtained for the wild-type enzyme (∼13 kcal/mol) when we use the Gaussian approximant to the barrier distribution is very close to the value of 13.4 kcal/mol derived from the experimentally measured rate constant of 950 s^{-1} for the hydride transfer.[4] This is unexpected, in light of the fact that PM3 is likely to be overestimating individual reaction barriers. It is possible that this occurrence is simply fortuitous. [In fact, the thermally averaged effective energy barrier is relatively insensitive to the positioning of the mean in the Gaussian representation of the barrier distribution. If we displace the mean ∼10 kcal/mol lower than that observed from the PM3-computed distributions, as could arise from the use of more accurate quantum chemical methods (see Table 2), the effective barrier changes by less than 50% and their relative orderings remain unaffected.] Consequently, the actual numerical value of these free-energy barriers should not be given too much weight. It is more important to recognize what the relative values of these energy barriers can tell us about the qualitative features of hydride transfer in DHFR. The free-energy barrier computed for G121V is greater than that of the wild-type protein, as we had expected. However, our calculations indicate that the free-energy hydride-transfer barrier itself is not significantly different for G121S compared to wild-type. Experimentally, G121S does exhibit a hydride-transfer rate that differs from that measured in the wild-type protein. This implies that the hydride-transfer barrier itself is not the primary cause of experimentally measured reaction rate differences between the G121S mutant and wild-type DHFR. For example, a reduced fraction of molecules occupying configurations conducive to the hydride transfer may be the source of the reduced hydride-transfer rate for this mutant. The

diminished occurrence of low hydrogen−acceptor distances in G121S relative to the other two proteins (see section 2.1) suggests a reduction in the equilibrium fraction of productive conformations for this mutant. However, more detailed analyses must be done before this can be conclusively shown. We are actively engaged in such efforts.

The reactivity of G121S compared to wild-type DHFR and G121V could also be due to other sources of rate differences in the three enzyme systems. Such features include the pK_a of position N5 of DHF and quantum dynamical effects (such as tunneling). The pK_a of position N5 will determine the fraction of enzymes at specific pH values containing protonated DHF and available to undergo the hydride transfer; this may be slightly different for the three protein systems. By protonating N5 in the current calculations, we have removed this factor from consideration and have only examined the hydride-transfer event itself. Consequently, the pH dependence of the hydride transfer is not relevant to the present study. This issue is explored in a recent paper from our group.[2]

The effect of protein motions on the rate of barrier recrossings for the hydride-transfer reaction could also affect relative reaction rates in the three proteins. Hammes-Schiffer and co-workers have shown that the incorporation of quantum dynamical effects should further reduce the barrier to hydride transfer by 2−3 kcal/mol.[12] The extent of this effect may differ for the three protein systems. Because of the nature of our calculations, we did not explore this issue.

4.3. Distinct Protein Substates are Mediated by the M20 Loop. Theoretical studies have indicated that the acceptor−donor distance, the angle between the donor, hydride, and acceptor, as well as the dihedral angle between the DHF pteridine and NADPH nicotinamide rings are important contributors to the global reaction coordinate.[5,32,49] In these studies, the hydride−acceptor distance in the transition state ranges from 1.4 to 1.6 Å, the angle between the acceptor, hydride, and donor carbons ranges from 155° to 180° and a value close to 0° for the dihedral angle between the pteridine and nicotinamide rings is energetically favored. The frequency of occurrence of low hydrogen−acceptor distances is different for the different protein isoforms (see section 2.1.), but this variation does not account for the experimentally measured differences in reaction rate for the three proteins. In addition, the frequency of occurrence of acceptor−hydrogen−donor and pteridine−nicotinamide dihedral angles within the ranges described above does not vary greatly between the wild type and the two mutants studied (data not shown). Thus, the activation energy for the reaction must also be a function of other features within the protein and solvent environment.

A key structural difference between the three protein isoforms that is immediately apparent is the interaction of residue 121 with surrounding residues. The results of NMR experiments[51] indicate that the conformation of DHFR in which the M20 loop occupies the "closed" conformation is the one most relevant to the occurrence of hydride transfer. As described by Sawaya and Kraut and displayed in crystal structure 1rx2 (see Figure 1), the center of the M20 loop forms a short β-sheet and type III′ hairpin turn that seals the active site in the closed conformation.[13] The nicotinamide ring is not thought to fully occupy the binding pocket unless the M20 loop is in a closedlike position. Residues within the M20 loop of the mutant proteins exhibit backbone dihedral angles not observed in wild-type DHFR (see Figure 4b). In particular, these alternate dihedral angle conformations correspond to M20 loop conformations that are less like the closed form.

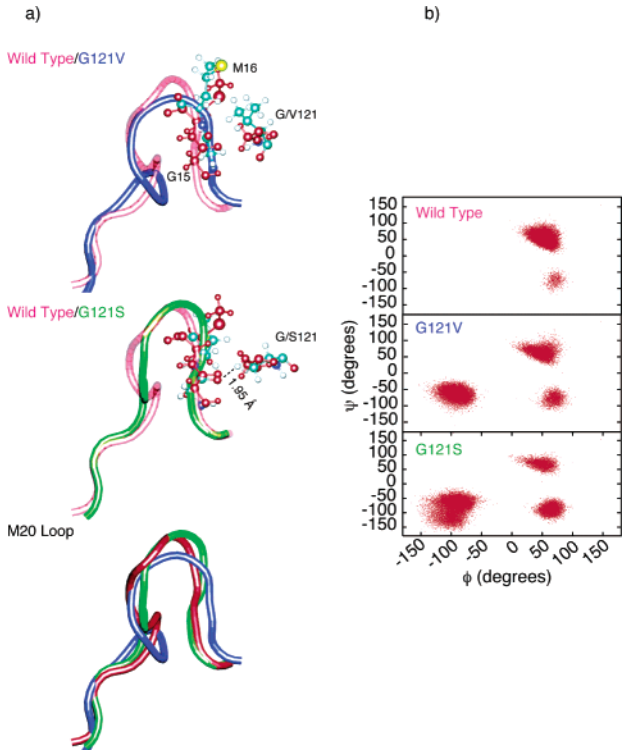

Figure 4. (a) Interactions of residue 121 with the M20 loop in the three protein systems. A tube representation of the peptide backbone from residues 14−24 is displayed. Residues 15, 16, and 121 are shown in atomic detail. The loops were aligned on the basis of the Cα positions of residues 13−16 and 22−25. In the top two illustrations, the M20 loop conformation from the mutants is compared with that from the native protein simulation (the superposition of all three is shown in the third illustration). The orientation shown here is rotated approximately 90° about the horizontal axis relative to Figure 1. The hydrogen bond made by the serine side chain at position 121 and glycine at 15 is indicated. (b) The distribution of backbone ϕ and ψ angles for residue 17 in the M20 loop of DHFR throughout the entire 10 ns trajectory for each enzyme isoform. The closed conformation of the M20 loop is that defined by dihedral angles found in the crystal structure 1rx2 and corresponds to $\phi \sim 25-75°$ and $\psi \sim 50-100°$ for this residue.

As can be seen in Figure 4a, residue 121 in DHFR interacts with the early part of the M20 loop (wild type). In G121V, the bulky side chain of valine 121 displaces glycine 15 and methionine 16, the two M20 loop residues contacting position 121. In G121S, the side chain hydroxyl of serine 121 forms a hydrogen bond to the backbone carbonyl of glycine 15 that is not possible in the wild type. Different interactions at position 121 modify M20 loop conformations in the three mutants. These alternate loop conformations may modulate the environment in the vicinity of the active site, leading to reduced activity in the mutants relative to the wild-type enzyme. The backbone dihedrals of M20 loop residues may be one component of a low energy conformational substate as discussed earlier.

4.4. Geometric Descriptors Correlated to Hydride-Transfer Progress. To further compare the results of this study with those presented by Hammes-Schiffer and co-workers,[12] we calculated the average change in interatomic distances between atoms in the reactive state and those in the transition-state configuration; these data are presented in Table A1. The average change of the geometric parameters is generally of the same sign as that seen by these researchers. Thus, our work reflects the general trends of correlation that they observe. While the percent average change is often less than that reported by Hammes-Schiffer and co-workers, this size difference is anticipated because the protein and much of the solvent were kept

fixed during our QM/MM calculations. However, there are certain instances where our results differ in the sign of the change observed. These differences may indicate that the changes of this small set of interatomic distances do depend on motion within the protein, as suggested by Hammes-Schiffer and co-workers. However, they may also indicate cases where the existence of local minima has obscured the true behavior of the enzyme system in the work of these researchers, or where conformations far from the transition-state region play a major role in the behavior of these features. When one examines Table A1, it is clear that there are several distances associated with progress along the reaction coordinate and that the reaction coordinate is a complex and collective entity. In light of this, the choice of specific coordinates to track the course of the reaction becomes problematic. With our distributions of hydride-transfer energy barriers in hand, we hope to use the low energy calculated barriers as an unbiased selection criterion for parameters associated with lowered hydride-transfer barriers.

To complete a discussion comparing the present study to that of Hammes-Schiffer and co-workers, we would like to comment on the source of the geometric correlation presented in Table A1. The coupling observed by these researchers is a measure of changes in the equilibrium conformations of the protein and cannot provide insight into whether these changes originate in the protein or are the result of rearrangements of the reactants within the active site. Since we observe many of the same trends as Hammes-Schiffer and co-workers while employing fixed protein systems, the impact of protein motions is unlikely to be the source of these correlations. In fact, these correlations must have their origin in the movements of groups within the reaction center. In addition, because the protein systems we employ are immobile, the structural and energetic trends we observe cannot be due to dynamic coupling. In other words, our results do not support the existence of a mechanism where time-dependent displacements of enzymatic groups directly contribute energy to the hydride-transfer process. While not explicitly proposed to be present in DHFR by Hammes-Schiffer and co-workers, this phenomenon has been suggested to exist for other enzymatic reactions.[20−22] If such dynamical coupling of protein modes to activity at the catalytic center is important for the enzymatic activity of DHFR, we would not expect to see any differences between the energies we compute employing immobile snapshots from the MD simulations. Yet, differences in the distributions of hydride-transfer energy barriers exist that qualitatively agree with differences in the experimentally determined rate constants. This indicates that it is the modulation of the conformational ensemble in the proteins that is the primary source of differences in the height of the barrier to hydride transfer and, consequently, reaction rate. The protein and solvent configuration are necessarily the main determinants of the height of the energy barrier for the hydride transfer, since these are the only features that change significantly with the different structures used in our calculations. Protein fluctuations are either important in establishing these structural ensembles or merely indicate that they have been modified. While this does not absolutely preclude the direct contribution of time-dependent protein displacements to reductions in the energy barrier for the reaction, any such direct dynamical coupling to the reaction rate must play a minor role. Our results indicate that preorganization of molecular groups or modulation of ground-state fluctuations of the ligands are the major factors in determining the reaction barrier for hydride transfer in DHFR.

5. Concluding Remarks

We have demonstrated that differences in energy barrier distributions exist for wild-type DHFR compared to the two mutants examined in this study, G121S and G121V. This work illustrates that the effects of mutations outside of the active site can be manifest in the energy barrier for an enzyme-catalyzed reaction and that these effects can be reproduced using available computational methods. At the time of writing, this was the first time that this had been established for a protein and its mutant variants. It is likely that the conformational ensemble of each DHFR variant contains unique features responsible for these energy distributions.

The variation in individual energy barriers that we observe is in accord with the results of experimental and theoretical studies demonstrating that energy barriers for enzyme-catalyzed reactions can fluctuate on a single molecule basis.[26,27] This situation is in contrast to the tenets of conventional chemical kinetics and is an important feature that must be taken into account for enzyme systems.[52] By using averages derived from our energy distributions, we obtain values for free-energy barrier differences among the three protein systems examined that agree qualitatively with experimental estimates. The free-energy barrier for G121V is greater than that for wild type, as we had expected on the basis of experimental rate measurements. In contrast, the barrier for G121S is close to that of wild-type DHFR. This may suggest that features other than the reaction barrier are the primary reason for rate differences between this mutant and the wild-type enzyme. These features could include effects such as the equilibrium fraction of molecules occupying configurations favorable to the hydride transfer, the pK_a of position N5 of DHF, or the action of enzyme motions in facilitating barrier re-crossings for the hydride transfer. Further studies are needed to elucidate the molecular basis for the observed differences in the effective energy barriers obtained. It is essential to establish which structural features are relevant to providing an environment conducive to hydride transfer and how these differ between the wild-type and mutant proteins.

Our work indicates that alteration of equilibrium conformational distributions rather than dynamical coupling is the key factor influencing the rate of hydride transfer in DHFR. Several distances in the enzyme systems studied change in a manner that is correlated with the course of the reaction. These changes originate from the progress of the reaction itself and are not the result of promoting motions in the protein. Coupling of enzyme motion to the reactive event occurs in the context of conformational changes that facilitate the hydride transfer. Such coupling is not truly dynamic as earlier defined (see sections 1 and 4.4), since time-dependent displacements of enzymatic groups do not directly contribute energy to induce the reactive event. This is strong evidence that the role of correlated motions in DHFR previously identified by Radkiewicz and Brooks[15] is to generate the correct conformational ensembles for efficient hydride transfer rather than to directly deliver energy from time-dependent protein displacements into the hydride-transfer process.

Acknowledgment. We acknowledge Dr. Thomas H. Rod and Professor Jennifer L Radkiewicz for their helpful discussions and sharing results of their unpublished calculations with us. Financial support for this work under funds from the National Institutes of Health (GM56879 and GM37554) is acknowledged. All computations were carried out on the TSRI supercomputing facilities.

Appendix

A.1. Structural Correlations during Hydride Transfer. The table below presents results for correlations between movement of reactants during the hydride-transfer reaction and specified atoms in the protein (or other portions of the reactants). The results demonstrate that several apparent correlations between protein motion and progress in the reaction occur and agree with earlier findings from Hammes-Schiffer and co-workers;[12] however, the protein environment is fixed in the present calculations. This suggests that the correlations arise from structural rearrangement of the reactants (DHF and NADPH) within the protein environment during hydride transfer and not from correlated movements of protein residues and the hydride transfer.

TABLE A1: Average Change of Distance between Selected Protein and Ligand Atoms in DHFR

atom 1	atom 2	% average change[a]	% average change[b]
donor	acceptor	−16.64	−21.74
ALA7-Cβ	DHF-N3	4.39	−0.57
ILE14-Cα	acceptor	−2.02	−4.77
ILE14-Cδ	donor	9.93	4.54
GLY15-Cα	acceptor	−4.40	−4.37
GLY15-Cα	DHF-N10	6.44	−1.90
ASP27-Oδ1	donor	−14.21	−0.58
ASP27-Oδ1	NADPH-NO7	−20.25	−1.74
ASP27-Oδ1	DHF-NA2	31.30	0.62
ASP27-Oδ2	DHF-N3	20.92	0.14
ASP27-Oδ2	NADPH-NO7	17.32	−1.83
LEU28-Cα	acceptor	9.83	3.04
LEU28-Cδ1	acceptor	17.87	3.22
LEU28-Cδ1	DHF-C	40.23	−0.83
LEU28-Cδ2	NADPH-NO7	−15.63	−1.67
PHE31-Cα	acceptor	11.30	3.94
PHE31-Cβ	acceptor	14.08	4.89
PHE31-Cζ	DHF-C11	−17.11	−1.65
PHE31-Cζ	acceptor	19.04	8.11
VAL40-Cα	acceptor	0.89	2.53
VAL40-Cβ	acceptor	−1.02	3.22
ILE41-Cδ	NADPH-AN7	−1.65	0.00
GLY43-Cα	acceptor	−1.21	−0.79
ARG44-Cα	acceptor	−4.03	−0.55
ARG44-Cβ	acceptor	−3.59	−0.59
ARG44-NH1	acceptor	−5.57	−0.91
ARG44-NH1	DHF-C9	−5.14	−0.19
THR46-Cα	acceptor	−8.18	−1.24
THR46-Cβ	acceptor	−7.62	−1.48
THR46-Oγ1	acceptor	−6.77	−2.87
THR46-Cγ2	DHF-C9	−6.98	0.36
TRP47-N	DHF-C9	−7.23	0.79
TRP47-Cα	acceptor	−7.24	0.72
TRP47-Cβ	acceptor	−5.73	0.69
LEU54-Cδ1	acceptor	8.87	5.47
LEU54-Cδ1	donor	4.94	−2.69
LEU54-Cδ1	DHF-C16	−12.49	3.47
LEU54-Cδ1	NADPH-NC5	5.81	−2.60
LEU54-Cδ2	DHF-CT	−34.28	−0.65
ILE61-CD	donor	−0.50	−1.51
LEU62-O	NADPH-AC1	0.48	0.02
LEU62-Cα	acceptor	−0.78	−0.02
LEU62-Cδ1	acceptor	−6.13	−0.038
LEU62-Cδ1	DHF-C7	−6.83	−0.04
LEU62-Cδ1	NADPH-AC5	−9.90	0.00
SER63-Oγ	donor	0.56	−0.39
TYR100-OH	acceptor	10.27	−5.79
TYR100-OH	donor	4.36	1.15
TYR100-OH	DHF-N8	16.54	−0.67
THR113-Cα	acceptor	1.73	−0.90
THR113-Oγ1	acceptor	2.89	−0.12
THR113-Oγ1	DHF-NA2	4.87	−0.31
ASP122-Cβ	acceptor	−1.42	−2.73

[a] From Agarwal et al.[12] [b] Results from this study. The percent average change for each distance was calculated as described in Agarwal et al.:[12] [(avg. dist. TS) − (avg. dist. reactant)]/(avg. dist. reactant).

References and Notes

(1) Stryer, L *Biochemistry*, 4th ed.; W. H. Freeman and Co.: New York, 1995.
(2) Rod, T. H.; Brooks, C. L., III. *J. Am. Chem. Soc.* **2003**, *125*, 8718−9.
(3) Cummins, P. L.; Gready, J. E. *J. Am. Chem. Soc.* **2001**, *123*, 3418−28.
(4) Fierke, C. A.; Johnson, K. A.; Benkovic, S. J. *Biochemistry* **1987**, *26*, 4085−92.
(5) Wu, Y.-D.; Lai, D. K. W.; Houk, K. N. *J. Am. Chem. Soc.* **1995**, *117*, 4100−8.
(6) Epstein, D. M.; Benkovic, S. J.; Wright, P. E. *Biochemistry* **1995**, *34*, 4, 11037−48.
(7) Miller, G. P.; Benkovic, S. J. *Chem. Biol.* **1998**, *5*, R105−13.
(8) Miller, G. P.; Wahnon, D. C.; Benkovic, S. J. *Biochemistry* **2001**, *40*, 867−75.
(9) Verma, C. S.; Caves, L. S.; Hubbard, R. E.; Roberts, G. C. *J. Mol. Biol.* **1997**, *266*, 776−96.
(10) Greatbanks, S. P.; Gready, J. E.; Limaye, A. C.; Rendell, A. P. *Proteins* **1999**, *37*, 157−65.
(11) Pan, H.; Lee, J. C.; Hilser, V. J. *Proc. Natl. Acad. Sci. U.S.A.* **2000**, *97*, 12020−5.
(12) Agarwal, P. K.; Billeter, S. R.; Hammes-Schiffer, S. *J. Phys. Chem. B* **2002**, *106*, 3283−93.
(13) Sawaya, M. R.; Kraut, J. *Biochemistry* **1997**, *36*, 586−603.
(14) Cameron, C. E.; Benkovic, S. J. *Biochemistry* **1997**, *36*, 15792−800.
(15) Radkiewicz, J. L.; Brooks, C. L., III. *J. Am. Chem. Soc.* **2000**, *122*, 225−31.
(16) Rod, T. H.; Radkiewicz, J. L.; Brooks, C. L., III. *Proc. Natl. Acad. Sci. U.S.A.* **2003**, *100*, 6980−5.
(17) Kraulis, P. J. *J. Appl. Cryst.* **1991**, *22*, 946−50.
(18) Benkovic, S. J.; Bruice, T. *Biochemistry* **2000**, *39*, 6267−74.
(19) Young, L.; Post, C. B. *Biochemistry* **1996**, *35*, 15129−33.
(20) Knapp, M. J.; Klinman, J. P. *Eur. J. Biochem.* **2002**, *269*, 3113−21.
(21) Antoniou, D.; Caratzoulas, S.; Kalyanaraman, C.; Mincer, J. S.; Schwartz, S. D. *Eur. J. Biochem.* **2002**, *269*, 3103−12.
(22) Cui, Q.; Karplus, M. *J. Phys. Chem. B* **2002**, *106*, 7927−47.
(23) Agarwal, P. K.; Billeter, S. R.; Rajagopalan, P. T. R.; Benkovic, S. J.; Hammes-Schiffer, S. *Proc. Natl. Acad. Sci. U.S.A.* **2002**, *99*, 2794−9.
(24) Rajagopalan, P. T. R.; Lutz, S.; Benkovic, S. J. *Biochemistry* **2002**, *41*, 12618−28.
(25) Watney, J. B.; Agarwal, P. K.; Hammes-Schiffer, S. *J. Am. Chem. Soc.* **2003**, *125*, 3745−50.
(26) Lu, H. P.; Xun, L.; Xie, X. S. *Science* **1998**, *282*, 1877−82.
(27) Zhang, Y.; Kua, J.; McCammon, J. A. *J. Phys. Chem. B* **2003**, *107*, 4459−63.
(28) MacKerell, A. D., Jr.; Brooks, B.; Brooks, C. L., III; Nilsson, L.; Roux, B.; Won, Y.; Karplus, M. CHARMM: The Energy Function and its Parameterization with an Overview of the Program. In *The Encyclopedia of Computational Chemistry*; Schleyer, P. v. R. e. a., Ed.; John Wiley and Sons: Chichester, U.K., 1998; Vol. 1, pp 271−7.
(29) Jorgensen, W. L.; Chandrasekhar, J.; Madura, J. D.; Impey, R. W.; Klein, M. L. *J. Chem. Phys.* **1983**, *79*, 926−35.
(30) Brooks, B. R.; Bruccoleri, R. E.; Olafson, B. D.; States, D. J.; Swaminathan, S.; Karplus, M. *J. Comp. Chem.* **1983**, *4*, 187−217.
(31) Andres, J.; Moliner, V.; Safont, S. V.; Domingo, L. R.; Picher, M. T.; Krechl, J. *Bioorg. Chem.* **1996**, *24*, 10−8.
(32) Castillo, R.; Andres, J.; Moliner, V. *J. Am. Chem. Soc.* **1999**, *121*, 12140−7.
(33) Amara, P.; Field, M. J. Hybrid potentials for large molecular systems. In *Computational Molecular Biology (Theoretical Computational Chemistry)*; Leszczynski, J., Ed.; Elsevier Science: Amsterdam, The Netherlands, 1999; Vol. 8, pp 1−33.
(34) Cummins, P. L.; Gready, J. E. *J. Mol. Graph. Modl.* **2000**, *18*, 42−9.
(35) Alhambra, C.; Corchado, J. C.; Sanchez, M. L.; Gao, J.; Truhlar, D. G. *J. Am. Chem. Soc.* **2000**, *122*, 8197−203.
(36) Gready, J. E. *Biochemistry* **1985**, *24*, 4761−6.
(37) Chen, Y.-Q.; Kraut, J.; Blakley, R. L.; Callender, R. *Biochemistry* **1994**, *33*, 7021−6.
(38) Deng, H.; Callender, R. *J. Am. Chem. Soc.* **1998**, *120*, 7730−7.
(39) Gao, J.; Amara, P.; Alhambra, C.; Field, M. J. *J. Phys. Chem.* **1998**, *102*, 4714−21.
(40) Tobias, D. J.; Brooks, C. L., III. *Chem. Phys. Lett.* **1987**, *142*, 472−6.
(41) Steinbach, P. J.; Chu, K.; Frauenfelder, H.; Johnson, J. B.; Lamb, D. C.; Nienhaus, G. U.; Sauke, T. B.; Young, R. D. *Biophys. J.* **1992**, *61*, 235−245.
(42) Garcia-Viloca, M.; Alhambra, C.; Truhlar, D. G.; Gao, J. *J. Chem. Phys.* **2001**, *114*, 9953−8.

(43) Frisch, M. J.; Trucks, G. W.; Schlegel, G. E.; Scuseria, G. E.; Robb, M. A.; Cheeseman, J. R.; Zakrzewski, V. G.; Montgomery, J. A., Jr.; Stratmann, R. E.; Burant, J. C.; Dapprich, S.; Millam, J. M.; Daniels, A. D.; Kudin, K. N.; Strain, M. C.; Farkas, O.; Tomasi, J.; Barone, V.; Cossi, M.; Cammi, R.; Mennucci, B.; Pomelli, C.; Adamo, C.; Clifford, S.; Ochterski, J.; Malick, D. K.; Rabuck, A. D.; Raghavachari, K.; Foresman, J. B.; Cioslowski, J.; Ortiz, J. V.; Baboul, A. G.; Stefanov, B. B.; Liu, G.; Liashenko, A.; Piskorz, P.; Komaromi, I.; Gomperts, R.; Martin, R. L.; Fox, D. J.; Keith, T.; Al-Laham, M. A.; Peng, C. Y.; Nanayakkara, A.; Challacombe, M.; Gill, P. M. W.; Johnson, B.; Chen, W.; Wong, M. W.; Andres, J. L.; Gonzalez, C.; Head-Gordon, M.; Replogle, E. S.; Pople, J. A. Gaussian 98, Revision A.10 ed.; Gaussian, Inc.: Pittsburgh, PA, 2001.

(44) Karpen, M. E.; Tobias, D. J.; Brooks, C. L, III. *Biochemistry* **1993**, *32*, 412−20.

(45) Schenter, G. K.; Lu, H. P.; Xie, X. S. *J. Phys. Chem. A* **1999**, *103*, 10477−88.

(46) Frauenfelder, H.; Sligar, S. G.; Wolynes, P. G. *Science* **1991**, *254*, 1598−603.

(47) Wang, J.; Wolynes, P. *J. Chem. Phys.* **1999**, *110*, 4812−9.

(48) Rajagopalan, P. T. R.; Zhang, Z.; McCourt, L.; Dwyer, M.; Benkovic, S. J.; Hammes, G. G. *Proc. Natl. Acad. Sci. U.S.A.* **2002**, *99*, 13481−6.

(49) Cummins, P. L.; Gready, J. E. *J. Comp. Chem.* **1998**, *19*, 977−88.

(50) Cummins, P. L.; Greatbanks, S. P.; Rendell, A. P.; Gready, J. E. *J. Phys. Chem. B* **2002**, *106*, 9934−44.

(51) Osborne, M. J.; Schnell, J.; Benkovic, S. J.; Dyson, H. J.; Wright, P. E. *Biochemistry* **2001**, *40*, 9846−59.

(52) Xie, X. S.; Lu, H. P. *J. Biol. Chem.* **1999**, *274*, 15967−70.